J. Ocean Univ. China (Oceanic and Coastal Sea Research)
https://doi.org/10.1007/s11802-019-3821-x
ISSN 1672-5182, 2019 18 (2): 261-270
http://www.ouc.edu.cn/xbywb/
E-mail:xbywb@ouc.edu.cn

Linkage Between Winter Temperatures in the Yellow Sea and Atmospheric Circulation Indices

YUAN Chengyi[1)], WEI Hao[2), *], LUO Xiaofan[2)], and KUANG Xiaodi[3)]

1) *College of Marine and Environmental Sciences*, *Tianjin University of Science and Technology*, *Tianjin* 300457, *China*
2) *School of Marine Science and Technology*, *Tianjin University*, *Tianjin* 300072, *China*
3) *National Marine Environmental Forecasting Center*, *Beijing* 100081, *China*

(Received February 5, 2018; revised April 20, 2018; accepted August 11, 2018)

Abstract This study investigated the linkage between winter temperature in the Yellow Sea (YS), China, and atmospheric indices and established this linkage through statistical models. The water temperature was obtained through hindcast simulation using a global–regional nested ocean model for the period of 1958–2007. The interannual variations of the simulated temperature were validated using satellite and *in-situ* observations. In the YS, the winter sea surface temperature (SST) had obvious interannual variations, with the maximum SST exceeding 2℃, and a significant shift from the cold to warm phase during 1988–1989. Based on the mechanism study, statistical models for the variations of water temperature in the YS were established using suitable atmospheric indices as predictors. For the northern YS (NYS) and the coastal region of the southern YS (SYS), statistical models of SST were established using linear regression based on the December–January–February mean Arctic oscillation index (AOI), representing the dominant large-scale atmospheric variability in boreal winter. For the YS warm current (YSWC) region, statistical models were established using both the AOI and the first principal component of the local wind stress curl (PC1-Curl), derived from the empirical orthogonal functions analysis. The PC1-Curl represents the influence of the local wind stress curl on the west-to-east shifts of the YSWC pathway. The applications proved that the models presented in this study have the ability to estimate winter temperatures in the YS within the recent years.

Key words water temperature; statistical model; interannual variations; atmospheric variability; empirical orthogonal function analysis

1 Introduction

As the main indicator of climate change, water temperature has profound regional impacts on the marine ecosystems (Pörtner *et al.*, 2001; Stenevik and Sundby, 2007; Chassé *et al.*, 2014; Xu *et al.*, 2017). Statistical models have been widely used to predict water temperature (Mann *et al.*, 2014; Wagawa *et al.*, 2015), and numerous atmospheric and oceanic indices have been tested as predictors in these models. Mechanism studies on the linkage between variations in water temperature and potential predictors of water temperature can provide vital tools in formulating these statistical models (*e.g.*, Klöwer *et al.*, 2014).

The Yellow Sea (YS), located at mid-latitude between China and the Korean peninsula, is a semi-enclosed marginal sea of the Northwest Pacific. Historical satellite and *in-situ* observations have clearly demonstrated that the YS' water temperature in winter has significant interannual variability (Zhang *et al.*, 2009; Wei *et al.*, 2010, 2013; Park *et al.*, 2015). Predicting water temperature in winter together with its interannual anomalies, as proposed in this study, is of great interest to local fishery and ecosystem management (Lin *et al.*, 2005; Sun *et al.*, 2014; Wang *et al.*, 2014; Zhou *et al.*, 2016).

In the coastal and shallow regions of the YS, the interannual variations of water temperature and heat content during winter are primarily controlled by those of the heat flux at the sea surface, which can be linked to the variations of the East Asian winter monsoon (EAWM) and Arctic oscillation (AO). A positive phase of AO results in weakened EAWM and less heat loss at the sea surface, leading to a positive temperature anomaly in this region (Chen *et al.*, 2003; Wang *et al.*, 2009a, 2009b; Wei *et al.*, 2013). Currently, the operational forecast model has higher skill in predicting the AO index (Kang *et al.*, 2014; Stockdale *et al.*, 2015). Thus, AO as the dominant large-scale atmospheric variable is a suitable predictor for the water temperature in the shallow regions.

In the deep YS trough (YST), the YS warm current (YSWC), as a northward mean flow, brings warm and saline water into the interior of the YS during winter

* Corresponding author. Tel: 0086-22-27409515
E-mail: hao.wei@tju.edu.cn

(Hsueh, 1988; Le and Mao, 1990; Yu *et al.*, 2010; Hu *et al.*, 2017). Significant interannual variabilities in the strength and pathway of the YSWC have been revealed by both in-situ observations and numerical simulations (Tang *et al.*, 2001; Yu *et al.*, 2010; Lin *et al.*, 2011). The local heat budget and zonal difference in water temperature are highly influenced by the lateral heat transport induced by the YSWC (Qiao *et al.*, 2011; Yuan, 2011). However, linkage between the interannual variability of water temperature and that of the YSWC has not been fully understood and quantified in this region, providing incentive for the mechanism study described herein. Although the significance of the YSWC on water temperature has been confirmed, observing or forecasting high-resolution YSWC velocity is not easy. To address this issue, more suitable predictors for the statistical models have been sought through this mechanism study.

When establishing the statistical model of water temperature, a large number of atmospheric and/or oceanic indices could be predictors. Thus, in this study, the essential predictors were selected based on clear cause-and-effect relationships derived from the physical mechanisms of interannual variations of water temperature in the different sub-regions of the YS. This paper is organized as follows. In Section 2, the interannual variations of simulated water temperature are validated for different sub-regions of the YS. In Section 3, spatial and temporal variations of the simulated sea surface temperature (SST) in winter are investigated; statistical models of winter temperatures are established for the coastal and shallow region and the YSWC region, respectively. In Section 4, the application of the statistical models and the associated potential usage for prediction are discussed. A summary of the study's findings is provided in Section 5.

2 Hydrodynamic Model Validation and Atmospheric Index Datasets

2.1 Hydrodynamic Model

The general ocean circulation model was based on version 2.3 of the Nucleus for European Modelling of the Ocean (http://www.nemo-ocean.eu/), including an ocean component and a sea-ice component. The water temperature was simulated using a two-way nested global-regional model. The regional model configured for the Northwest Pacific has a nominal horizontal resolution of 1/4˚ and a maximum of 46 levels in the vertical. The model forcing was adopted from version 2 of the atmospheric forcing dataset created for the common ocean-ice reference experiment (hereafter called CORE; Large and Yeager, 2004, 2009).

The model was first run for 10 years using the 'normal year forcing' of CORE, representing the climatology of the reanalysis period. The temperature fields analyzed here were simulated for the period of 1958–2007 using interannually varying atmospheric forcing, continued from the end of the spin-up. More details of the setup of this model and some basic validations were provided by Wei *et al.* (2013).

2.2 Validation of Interannual Variations of Water Temperature

The interannual variations of water temperature are validated for the typical sub-regions and stations shown in Fig.1. The sub-regions of the northern YS (NYS) and the western coastal region of the southern YS (SYS) are mainly <50 m deep. The thermal conditions in these regions are primarily controlled by the surface heat flux in winter (Wei *et al.*, 2013). The sub-region of the YSWC mainly locates in deep YST, where the water temperature is directly influenced by lateral heat transport (Qiao *et al.*, 2011). *In-situ* stations A (35.80˚N, 123.60˚E) and B (37.75˚N, 123.75˚E) are located in the central and northern parts of the YS, respectively. The remote-sensing SST of the advanced very high-resolution radiometer (AVHRR, noaasis.noaa.gov/NOAASIS/ml/avhrr.html) and ship-based observations of the sea surface and bottom temperatures obtained from archives maintained by the State Oceanic Administration of China were used to validate the above mentioned sub-regions and stations.

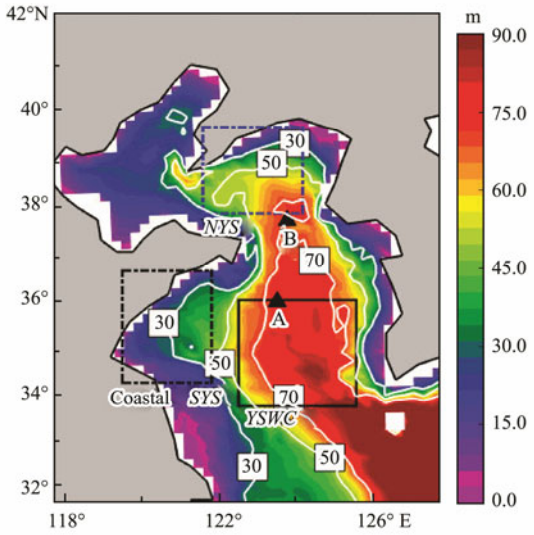

Fig.1 Topography of the Yellow Sea (YS). White contours with values marked in boxes denote isobaths of 30, 50 and 70 m. Color shading represents the topography in meters. The Yellow Sea warm current (YSWC) region and western coastal region in the southern Yellow Sea (coastal SYS) are marked by black solid and black dashed–dotted rectangles, respectively. The sub-region of the northern Yellow Sea (NYS) is marked by a blue dashed–dotted rectangle. *In-situ* stations A and B are marked by black triangles.

The statistics including correlations and root-mean-square (RMS) differences between the time series of the simulated and observed water temperatures in February were calculated according to the formulas in Taylor (2001) and are shown in Table 1. As a reference, the standard deviations of the simulated water temperature were also calculated. For various sub-regions, high correlations

were found between the time series of the area-averaged simulated SST and that of the satellite-observed SST in winter. The correlations reached almost 0.8 in the sub-regions of the YSWC and the NYS and even exceeded 0.9 in the coastal region of the SYS. For hydrographic stations, most correlations exceeded 0.85, except $r=0.7$ at the bottom of station B during winter. Note that the time series of the observed bottom temperature at station B is not quite continuous owing to missing data values. All RMS differences between the time series of simulated and observed SST were less than 0.6℃. Thus, such high correlations and reasonable RMS differences suggest that the hindcast simulation is suitable for investigating the linkage between the interannual variations of winter temperature and those of atmospheric forcing, thereby establishing the statistical models.

Table 1 Validation of the simulated water temperature in winter using observations based on statistics including correlation coefficient, RMS difference, and standard deviation

	Correlation coefficient	RMS difference (℃)	Standard deviation (℃)
SST-NYS	0.77	0.50	0.62
SST-Coastal SYS	0.90	0.34	0.77
SST-YSWC	0.79	0.40	0.57
SST-A	0.90	0.47	1.80
SST-B	0.85	0.58	1.05
BT-A	0.70	1.30	1.10
BT-B	0.89	0.90	1.50

Notes: Time series of the AVHRR SST and the ship-based water temperature observations were used for the sub-regions and *in-situ* stations, respectively, as shown in Fig.1. All correlations in this table are significant at 99% confidence level.

2.3 Atmospheric Circulation Index Datasets

The AO and its hemispheric equivalent, the North Atlantic oscillation (NAO), dominate the climate variability during winter in the Northern Hemisphere (Hurrell, 1995; Thompson and Wallace, 1998, 2000). The Arctic Oscillation Index (AOI) (available at http://tao.atmos.washington.edu or www.cpc.ncep.noaa.gov) is characterized by sea level pressure anomalies of one sign in the Arctic and the opposite sign centered at 37°–45°E. In this study, the December–January–February (DJF) mean of the AOI was used to represent the winter conditions during 1958–2007.

The reanalysis fields of the ERA-Interim 10 m wind speed with a resolution of approximately 25 km (http://apps.ecmwf.int/datasets/data/interim-full-daily) were produced and archived by the European Center for Medium-Range Weather Forecasts. The ERA-Interim dataset has been updated in a timely manner and also has better temporal coverage, which is helpful in the validation of statistical models of water temperature for the most recent years. The wind stress fields were calculated using piecewise functions of wind speed as described by Large and Pond (1981). Furthermore, leading empirical orthogonal function (EOF) modes of the winter wind stress curl were extracted for the periods of 1959–2007 and 1980–2014 while establishing the statistical models in Section 3 and for model applications in Section 4, respectively.

3 Statistical Model of Water Temperature

3.1 Climatology and Interannual Variations of the Simulated Temperature

The climatology of SST in February was derived by averaging the hindcast solution from 1958–2007. Fig.2a shows the contours of the climatology of SST in February. The spatial pattern of the contours indicates that a tongue of relatively warm water intrudes into the central YS mainly through the YST, which is closely related to the YSWC. Due to the significant heat loss at the sea surface and the lack of direct lateral heat input, the sub-regions of the NYS and the coastal SYS are about 7℃ and 6℃ cooler than the YSWC region, respectively.

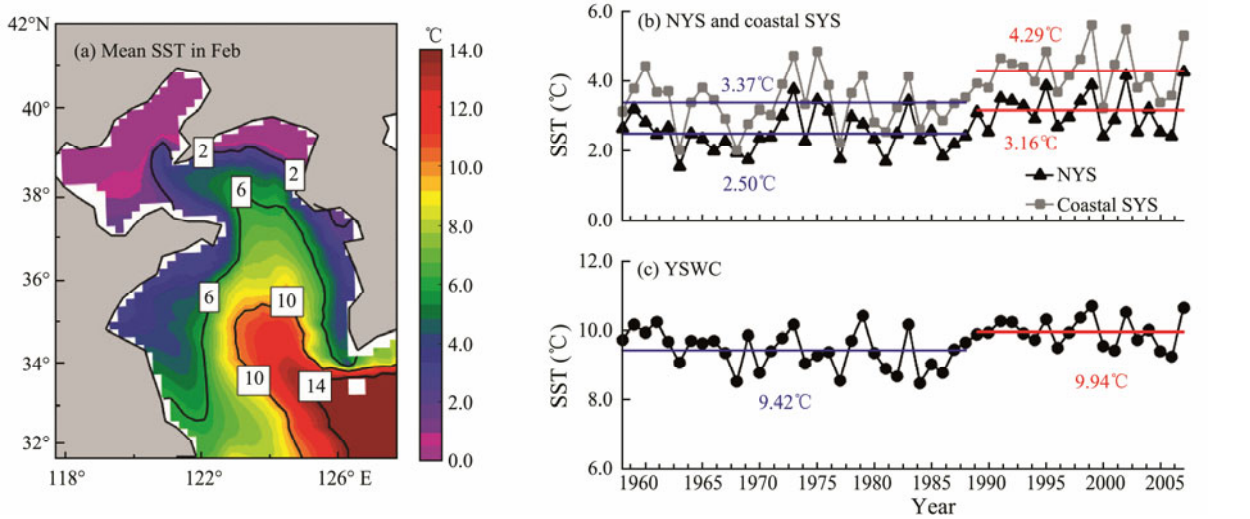

Fig.2 (a) Distribution of the model-simulated sea surface temperature (SST) in February in the YS. Time series of SST in February averaged over (b) the NYS and the coastal SYS and (c) the YSWC region. In (b) and (c), numbers in blue and red denote the winter SST averaged over the cooler and warmer periods of 1958–1988 and 1989–2007, respectively.

Fig.2b shows the time series of simulated SST in winter for the NYS and the coastal SYS. These two time series were highly correlated, with $r=0.93$. For each region, the 50-year time series can be divided into a cold phase of 1958–1988 and a warm phase of 1989–2007. During the cold phase, the mean SSTs in the NYS and the coastal SYS were 2.50℃ and 3.37℃, respectively. During the warm phase, the mean SSTs were 3.16℃ and 4.29℃, respectively. In general, the interannual variations and warming trends in the simulated SST in these regions were in agreement with those of the observed SST in the YS during 1976–2000, reported by Lin *et al.* (2005). The time series of the simulated winter SST in the YSWC region was less correlated with those in the NYS and the coastal SYS, with $r=0.68$ (Fig.2c). During the cold and warm phases, the mean SSTs were 9.42℃ and 9.94℃, respectively. From the cold to the warm phase, a shift of 0.52℃ was found, which was weaker than those simulated in the shallow and coastal regions.

3.2 Linkage to AOI in the Shallow Regions

Most coastal regions in the YS are less than 50 m deep (Fig.1). In these shallow regions, the thermal conditions are primarily controlled by the sea surface heat flux and are impervious to the lateral heat transport of the YSWC (Wei *et al.*, 2013). Thus, their response to atmospheric forcing is more significant as compared with that of the much deeper YST. Aiming to investigate the response of the local water temperature to large-scale atmospheric circulation, the correlation coefficients between the interannual variations of SST in February and those of the DJF-mean of AOI during 1958–2007 were calculated. We should mention here that the water temperature in February represents the final state of ocean thermal conditions controlled by sea-surface cooling and reflects the corresponding strength of AO in these shallow regions.

Fig.3 depicts the relatively high correlations between the SST in February of shallow regions in the YS and the DJF-mean of the AO index during the period of 1958–2007. SST in the NYS and western coastal region of the SYS had positive correlations ($r=0.56$ and $r=0.50$) with AOI. Hereinafter, all correlations were significant at 99% confidence level. For the eastern coastal region in the SYS, the temperature anomalies in February also suggested the highest correlation with AOI ($r=0.45$) among multiple climate indices using Korea Oceanographic Data Center datasets for the period of 1967–2008 (Park *et al.*, 2011). During the positive phase of AO, the strength of the EAWM prevailing over the YS is significantly weakened due to a weakened East Asia trough (Wang *et al.*, 2009a, 2009b). The weakening of the EAWM leads to less heat loss at the sea surface and higher water temperatures in the shallow regions. Thus, based on this physical mechanism, the statistical models can be established for the shallow regions of the YS.

Figs.4a and 4b illustrate the statistical models for winter SST during 1958–2007 in the NYS and the western region of the SYS, respectively. In these models, the time series of SST were reconstructed via linear regression analysis using AOI (Fig.4c), as shown in Eqs. (1) and (2). The reconstructed and modeled time series of SST during February were correlated at $r=0.61$ and $r=0.50$ in the NYS and the western region of the SYS, respectively. The amplitudes of the reconstructed temperature variations were underestimated due to the unexplained variance in the least square linear regression. Overall, the reconstructed time series captured most interannual variations in SST in the NYS and the western region of the SYS, except for some periods, such as 1979–1982.

$$SST_{\mathrm{NYS}} = 3.6\times10^{-1}\times AOI + 3.4\,, \tag{1}$$

$$SST_{\mathrm{SYS}} = 3.9\times10^{-1}\times AOI + 3.9\,. \tag{2}$$

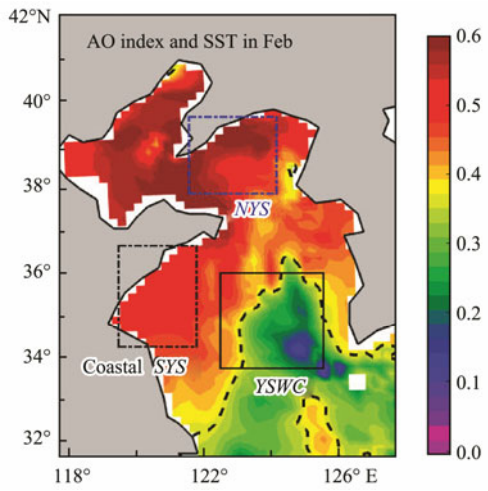

Fig.3 Correlation coefficients between interannual variations of SST in February and the DJF-mean of the AO index during 1958–2007. The correlations are significant at 0.05 levels except in regions inside the dashed contours. The sub-regions are the same as Fig.1.

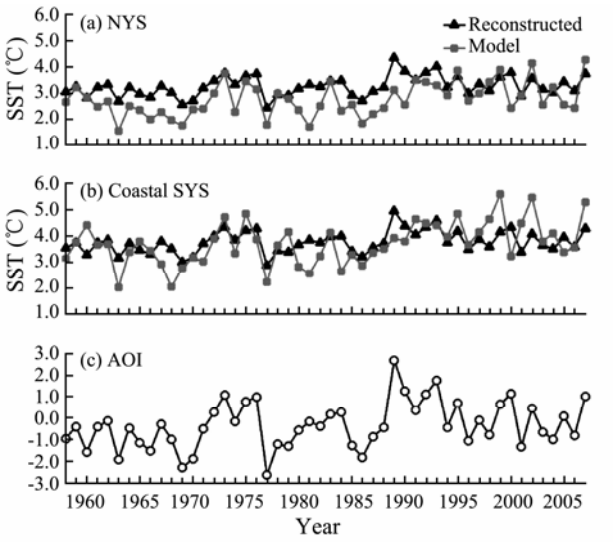

Fig.4 Time series of the reconstructed SST in (a) the NYS and (b) the coastal SYS derived from (c) the AO index and modeled temperature in February during 1958–2007.

3.3 Linkage to Atmospheric Indices in the YSWC Region

In the YSWC region (33.75°–36.00°N, 122.50°–125.50° E), the simulated water temperature in winter exhibited an insignificant or relatively low correlation with AOI during 1958–2007 (Fig.3). Moreover, EOF analysis of the long-term Pathfinder SST in winter exhibited an obvious east/west dipole pattern in this region (Song *et al.*, 2009), instead of a coherent pattern that could be attributed to the variability of AO. This dipole pattern of water temperature can be attributed to the east/west-ward shift of the YSWC pathway, which is induced by the interannual variability of the local wind stress curl in the central YS (Yuan, 2011). Thus, in addition to surface heat flux, the lateral heat transport related to the YSWC pathway is also an important factor contributing to the water temperature in this region.

To investigate the linkage between water temperature in this region and atmospheric circulation, EOF analyses were conducted to extract the principle modes of water temperature, the meridional velocity of ocean current, and the wind stress curl averaged over the period of the previous term of November to March. Typically, northward YSWC occurs during the term of the previous November to March in this hindcast simulation spanning the period of 1958–2007. Hence, this period was chosen to reflect the influence of the YSWC on the lateral heat transport and associated water temperature during its existence. To investigate the overall influence of lateral heat transport, temperature data was vertically averaged. At each location, the mean value was removed from the time series of the water temperature before performing the EOF analysis.

In the EOF analysis of the water temperature, the first and second EOF modes account for 59.7% and 28.8% of the total variance, respectively. EOF1-T exhibits a uniform sign, which indicates coherent warming or cooling over the YSWC region (Fig.5a). The mechanism study suggested that AO influences water temperature through both surface heat flux and the lateral heat transport related to the overall strength of the YSWC (Yuan, 2011; Wei *et al.*, 2013). PC1-T has a weak but significant correlation (r=0.33) with AOI. The time series of PC1-T and DJF-mean AOI during 1959–2007 showed similar dominant periods of 4–8 years and 12–20 years, respectively, identified *via* spectral analysis. Furthermore, the upward shift in PC1-T (Fig.5c) from the late 1980s corresponds to the AOI phase shift from negative to positive (Fig.4c). Hence, AOI was chosen as the predictor for the interannual variability of PC1-T.

EOF2-T presented an east-west dipole structure in the YSWC region, with the zero contour located at 123.5°–125.5°E (Fig.5b). The dipole pattern of EOF2-T can be explained by the east/west-ward shift of the YSWC pathway, which is represented by the EOF1-V derived from the EOF analysis on meridional velocity (Fig.6a). The westward shift of the YSWC leads to more lateral heat transport and favors an increase in temperature on the western flank of the YST. The opposite occurs during the eastward shift of the YSWC. The interannual variations of the YSWC pathway are controlled by the wind stress curl through the vorticity balance (*e.g.*, Lu and Stammer, 2004). The EOF1-Curl is the leading mode derived from the EOF analysis of the wind stress curl and accounts for 77.5% of the total variance (Fig.6b). The PC1-Curl showed a very high and positive correlation of r=0.91, with PC1-V associated with the YSWC pathway (Fig.6c). To evaluate the PC1-Curl as a potential predictor for water temperature, the time series of PC2-T and PC1-Curl are compared in Fig.7. They are highly correlated at r=0.76 during 1959–2007. The positive PC1-Curl corresponds to the

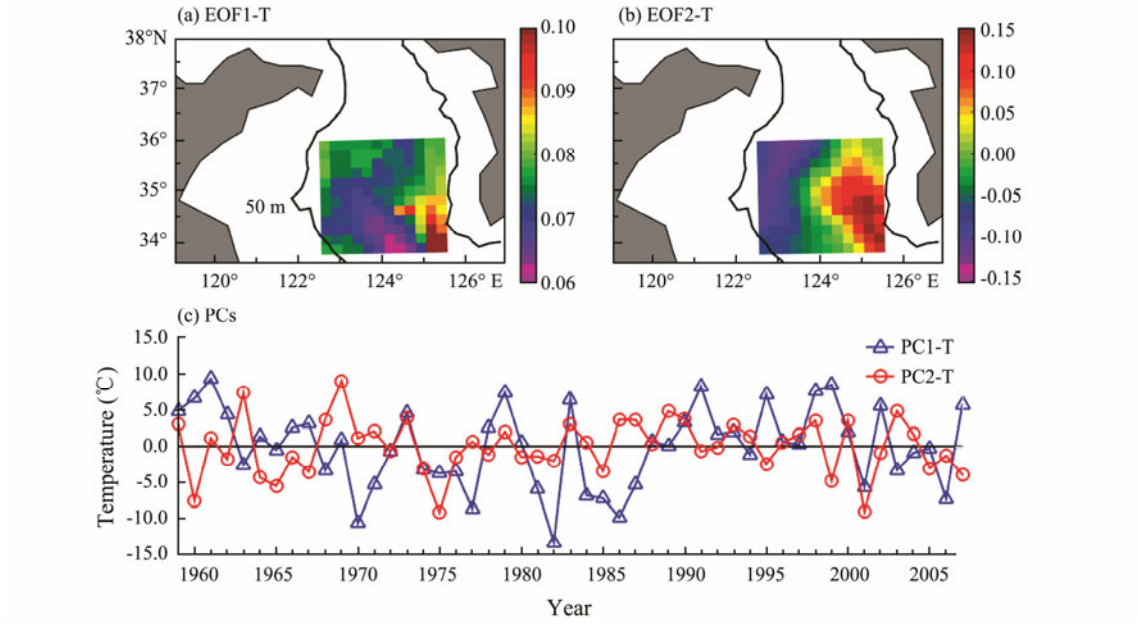

Fig.5 Spatial structures of (a) the first and (b) second EOF modes of the depth-averaged temperature during the winters (previous November to March) of 1959–2007, with the 50 m isobath represented using black curves. Panel (c) shows the time series of PC1 and PC2.

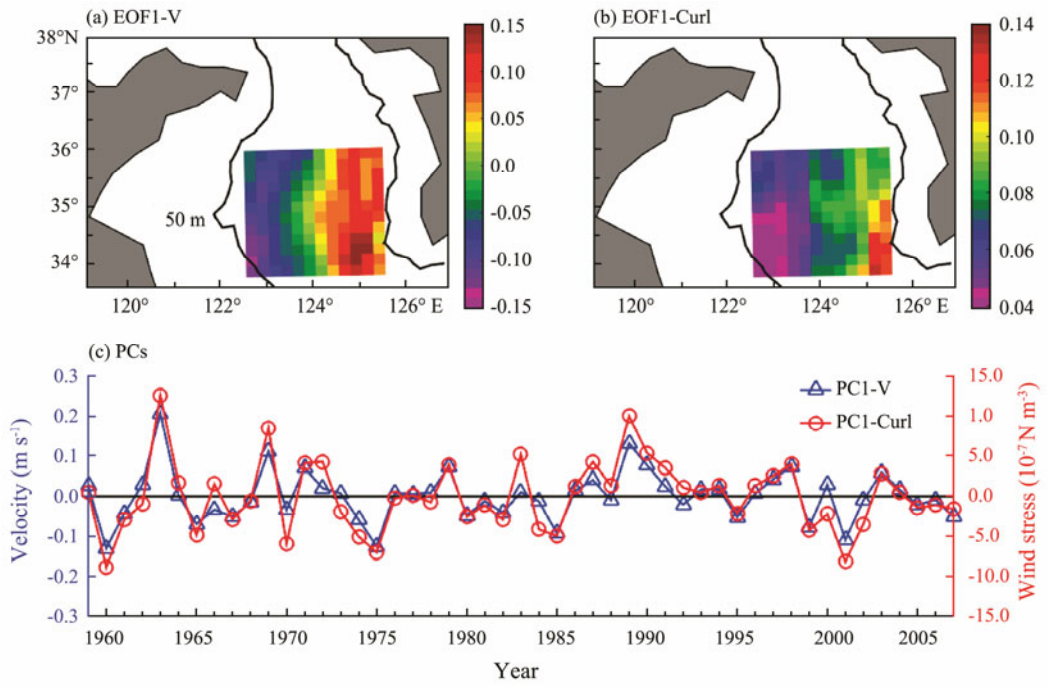

Fig.6 Spatial structures of the first EOF modes of (a) the depth-averaged meridional velocity and (b) the curl of the wind stress during the winters (previous November to March) of 1959–2007. The 50-m isobath is represented using black curves. Panel (c) shows the corresponding PC time series.

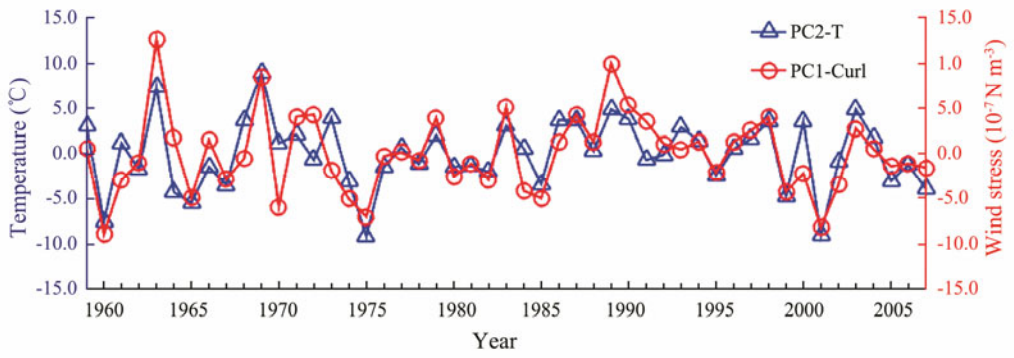

Fig.7 Time series of PC2-T and the PC1-Curl derived from the EOF analysis of the winter-mean water temperature and the wind stress curl during 1959–2007, respectively.

eastward shift of the YSWC pathway, causing an increase in temperature on the eastern flank, and vice-versa. Thus, EOF2-T can be further linked to the PC1-Curl, which is deemed a local atmospheric index in the YSWC region.

In brief, the coherent variations of the depth-averaged water temperature in the YSWC region are linked to large-scale atmospheric circulation through AOI, and the dipole variations of the water temperature are linked to local atmospheric circulation through the PC1-Curl.

3.4 Statistical Model for the YSWC Region

This investigation of the relationship between water temperature and atmospheric indices in the YSWC region suggests that the large-scale AO and the curl of the local wind stress are responsible for the first two EOF modes of the water temperature. Based on the statistics and mechanism analysis, the time series of the water temperature on the eastern (124.0˚–125.5˚E) and western (122.5˚–124.0˚E) flanks were reconstructed through multiple regression analysis using AOI and normalized PC1-Curl. Eqs. (3) and (4) show their statistical models. The reconstructed and model time series of the depth-averaged temperature during winter were correlated at $r=0.56$ and $r=0.50$ on the eastern and western flanks of the YST, respectively (Fig.8). Due to the unexplained variance in the least square linear regression, the amplitudes of the reconstructed temperature variations on the eastern flank of the YST were underestimated; *i.e.*, the reconstructed time series of the temperature captured most of the interannual variations on the eastern and western flanks of the YST.

$$T_{\text{Eastern}} = 1.6\times10^{-1}\times AOI + 2.3\times10^{-1}\times PC1-Curl + 12.0\,, \tag{3}$$

$$T_{\text{Western}} = 2.1\times10^{-1}\times AOI - 1.4\times10^{-1}\times PC1-Curl + 13.0\,. \tag{4}$$

Eqs. (3) and (4) show that regression coefficients associated with AOI were positive on both flanks of the YST, which indicates that high AOI favors an overall increase in water temperature in the YSWC region. In Fig.9a, the coefficients associated with AOI exhibit the same sign on both flanks. The high AOI, accompanied by a weakened EAWM and YSWC, induced less heat loss at the sea surface and less heat input from the lateral boundary. The coefficients tended to be larger on the western flank of the YST (Fig.9a). Thus, the influence of AO on water temperature is more important on the western flank, where the water depth is relatively shallower than that on the eastern flank.

Regression coefficients associated with the PC1-Curl showed different signs on the eastern and western flanks of the YST (Fig.9b), suggesting that the wind stress curl has opposite contributions to water temperatures on these two flanks. Consistent with the spatial distribution, the mean coefficients associated with the PC1-Curl have opposite signs in Eqs. (3) and (4). A positive PC1-Curl corresponding to positive anomalies of the local wind stress curl leads to eastward deviation of the YSWC pathway, which favors an increase in water temperature on the eastern flank with a decrease on the western flank, and vice-versa. In Fig.9b, the coefficients associated with the PC1-Curl are close to zero at 124.0°E, indicating that the role of the wind stress curl can be ignored at the mean location of the YSWC pathway.

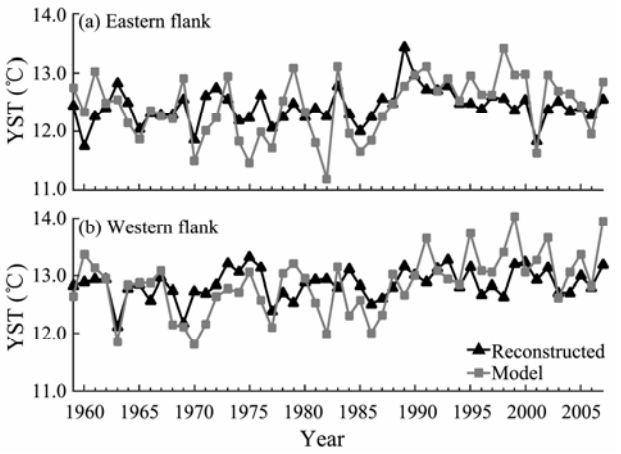

Fig.8 Time series of the reconstructed and modeled depth-averaged temperature on the (a) eastern and (b) western flanks of the YST during the winters of 1959–2007.

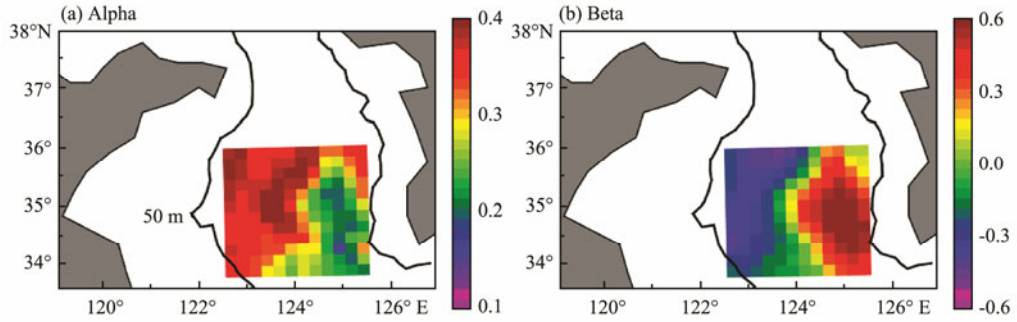

Fig.9 Spatial structures of coefficients derived from the multiple regression analysis of winter temperatures during 1959–2007 including (a) alpha associated with AOI and (b) beta associated with the PC1-Curl.

3.5 Relative Contributions of the AO and the Wind Stress Curl

To quantify the relative contributions of local and remote forcing on water temperature in the YSWC region, the ratios of the wind stress curl term and the AO term in Eqs. (3) and (4) were calculated for each location at 35°N on the two flanks of the YST (Fig.10a). On the eastern flank, the wind stress curl had more significant influence than that of AO on the interannual variations of the water temperature, with the averaged ratios being larger than 1.0 over 34 years and even larger than 2.0 over 18 years (Fig.10b). On the western flank, AO played a more important role in the interannual variations of temperature, with the averaged ratios being smaller than 1.0 over 29 years (Fig.10c).

At 35°N, the time series of the winter-mean temperature within different sub-regions were normalized for the period of 1959–2007. The winter-mean temperature in each year was normalized using Eq. (5):

$$X_{\text{norm}} = \frac{X_i - \overline{X_i}}{\sqrt{\dfrac{\sum_{i=1}^{n}(X_i - \overline{X_i})^2}{n}}}, \tag{5}$$

where X_i is the winter-mean temperature in each year, $\overline{X_i}$ is the temporal mean of water temperature during the period 1959–2007, n is the total year number, and X_{norm} is the corresponding normalized temperature.

The normalized time series exceeding 1.0/−1.0 were regarded as extreme warm/cold years, respectively. As shown in Table 2, 90% of the extreme cold years occurred in the western coastal region of the SYS, coinciding with those on the western flank of the YST. Due to the relative shallow water depth, half of these extreme cold years corresponded to the low AOI case. The occurrences of extreme cold and warm years showed fewer similarities on the eastern and western flanks of the YST due to the opposite role of the wind stress curl.

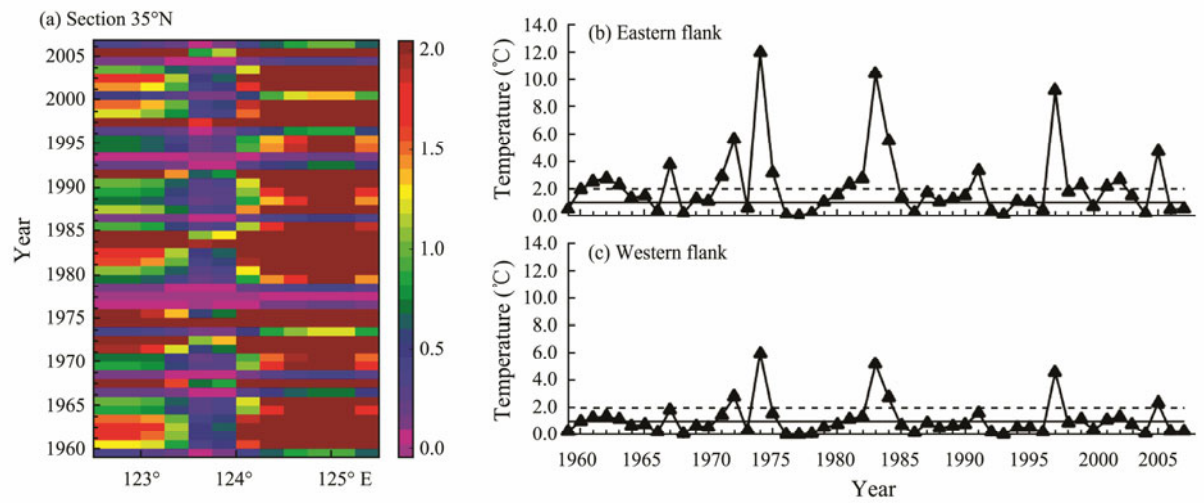

Fig.10 Ratios of the contributions of the wind stress curl and AO on the winter-mean temperature in the YSWC region (a) for each location at 35˚N and averaged over the (b) eastern and (c) western flanks, separated by 124˚E during 1959–2007.

Table 2 Extreme warm- and cold-year classifications based on the winter-mean temperature in the western coastal area of the SYS and on the eastern and western flanks of the Yellow Sea (YS) trough at 35˚N during 1959–2007

	Warm years	Cold years
Western coastal region of the SYS	1960, 1991, 1995, 1999, 2001, 2002, **2007**	**1963**, 1967, 1968, **1970**, **1977**, 1981, 1982, **1986**
Eastern flank of the YST	1969, **1973**, 1979, 1983, **1990**, 1991, 1998, **2000**	1964, 1965, **1970**, 1975, **1977**, 1981, 1982, 1985, 2001
Western flank of the YST	1991, 1995, 1999, 2002, 2005, **2007**	**1963**, 1967, 1968, **1969**, **1970**, 1971, **1977**, 1982, 1984, **1986**

Note: Bold numbers denote warm or cold years showing consistency with the positive or negative AO index.

4 Discussion

4.1 Application of Statistical Model

To evaluate the statistical models, time series of water temperature were constructed using these models for the periods of 1960–2014 and 1980–2014 for the coastal and the YSWC regions, respectively. For the NYS and the western region of the SYS, the SST time series were reconstructed using the DJF-mean of the monthly AOI by following Eqs. (1) and (2). For the western and eastern flanks of the YSWC region, the depth-averaged temperature time series were reconstructed using the PC1-Curl derived from the EOF analysis on ERA-Interim data and the DJF-mean of the monthly AOI according to Eqs. (3) and (4).

For the NYS and the coastal SYS regions, statistical models of winter temperature captured most of the interannual variations of the observed temperature (Fig.11). During 1960–2001, significant correlations of $r=0.53$ and $r=0.52$ were found between the time series of the reconstructed SST and the observed SST at two representative hydrological stations, A and B, respectively. During 1982–2014, significant correlations with $r=0.56$ and $r=0.50$ were also found between the reconstructed SST and the AVHRR SST averaged over two shallow regions, respectively. In addition, for the YSWC region, the reconstructed depth-averaged temperatures during 1980–2014 were correlated with the AVHRR SST at $r=0.48$ and $r=0.39$ on the eastern and western flanks of the YST, respectively (Fig.12). On these two flanks, even higher correlations with $r=0.70$ and $r=0.60$ were found between the time series of the reconstructed temperature and the AVHRR SST within the more recent period of 2000–2014.

The applicability of the atmospheric circulation indices in predicting winter water temperature was confirmed through the application of these statistical models, although some differences between predicted and observed temperature time series did exist.

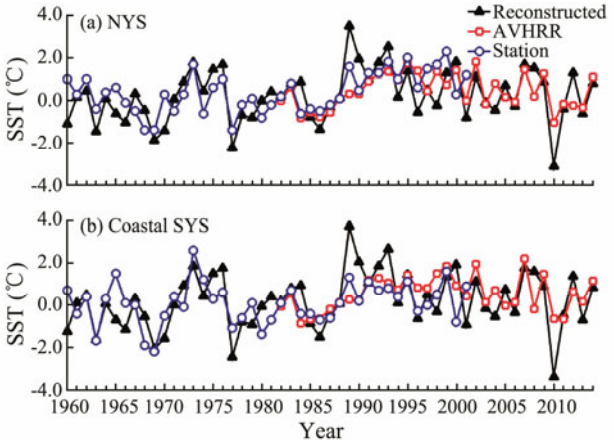

Fig.11 Time series of the reconstructed SST, the subdomain averaged AVHRR SST, and the SST recorded by the representative hydrological stations for the sub-regions of (a) the NYS and (b) the coastal SYS for winters during 1960–2014.

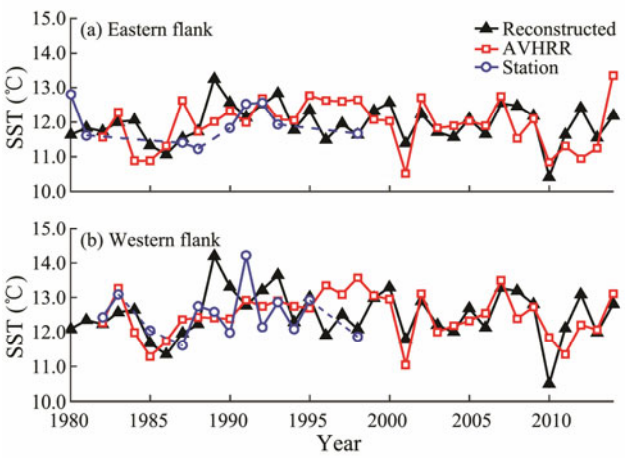

Fig.12 Time series of the reconstructed depth-averaged water temperature, sub-domain averaged AVHRR SST, and the SST recorded by the representative hydrological stations for the (a) eastern and (b) western flanks of the YST during the winters of 1980–2014.

4.2 Potential for Prediction Using AOI

For the shallow regions of the YS, statistical models of the water temperature have been established via linear regression using the DJF-mean AOI. Scaife *et al.* (2014) reported that wintertime AO and NAO can be forecasted for lead times exceeding two or more months using dynamic ensemble prediction systems. Furthermore, water temperature can be predicted for similar lead times using the forecasted AOI as the predictor in statistical models for the shallow regions of the YS. Predicting water temperature in winter can provide basic information for the management of fishery and marine ecosystems.

For the YSWC region, statistical models for winter temperature were established using AOI, which represented large-scale atmospheric circulation, and the PC1-Curl, which represented local atmospheric circulation. Due to the shallower water depth, AO plays a more significant role in both the interannual variations of water temperature and the occurrence of extreme cold years on the western flank.

5 Summary

Based on the hindcast simulation of the water temperature in the YS using a nested global-regional ocean model, two key questions were addressed in this research: 1) the linkage between water temperature and atmospheric circulation indices during winter and 2) the validity of the proposed statistical models for water temperature using atmospheric indices derived from different mechanisms for the shallow and the YSWC regions.

Notably, this ocean model has a relatively coarse resolution and does not explicitly include tides. The accuracy of the estimated interannual variations of water temperature should be further refined by increasing the resolution of the ocean model and atmospheric forcing. This method of establishing a statistical model of interannual variations in the hydrographic properties based on mechanism studies can also be applied to other marginal seas.

Acknowledgements

We acknowledge the support of the National Basic Research Program of China (973 Program) (No. 2011CB403606), the Tianjin Science and Technology Program (No. 14JCQNJC09900), and the National Natural Science Foundation of China (Nos. 41606028, 41376112). We also appreciate the anonymous reviewers who provided insightful and constructive comments on this study.

References

Chassé, J., Lambert, N., Comeau, M., Galbraith, P. S., Larouche, P., and Pettipas, P. G., 2014. Environmental conditions in the southern Gulf of St. Lawrence relevant to lobster. In: *DFO Canadian Science Advisory Secretariat Research Document*. Fisheries and Oceans Canada, Ontario, Ottawa, 1-25.

Chen, W., Takahashi, M., and Graf, H. F., 2003. Interannual variations of stationary planetary wave activity in the northern winter troposphere and stratosphere and their relations to NAM and SST. *Journal of Geophysical Research*, **108** (D24): 4797, DOI: 10.1029/2003JD003834.

Hsueh, Y., 1988. Recent current observations in the eastern Yellow Sea. *Journal of Geophysical Research*, **93** (C6): 6875-6884, DOI: 10.1029/JC093iC06p06875.

Hu, Z. F., Wang, D. P., He, X. Q., Li, M. T., Wei, J., Pan, D. L., and Bai, Y., 2017. Episodic surface intrusions in the Yellow Sea during relaxation of northerly winds. *Journal of Geophysical Research*, **122** (8): 6355-6546, DOI: 10.1002/2017JC012830.

Hurrell, J. W., 1995. Decadal trends in the North Atlantic Oscillation: Regional temperatures and precipitation. *Science*, **269** (5224): 676-679.

Kang, D., Lee, M., Im, J., Kim, D., Kim, H. M., Kang, H. S., Schubert, S. D., Arribas, A., and MacLachlan, C., 2014. Prediction of the Arctic Oscillation in boreal winter by dynamical seasonal forecasting systems. *Geophysical Research Letters*, **41** (10): 3577-3585, DOI: 10.1002/2014GL060011.

Klöwer, M., Latif, M., Ding, H., Greatbatch R. J., and Park, W., 2014. Atlantic meridional overturning circulation and the prediction of North Atlantic sea surface temperature. *Earth and Planetary Science Letters*, **406**: 1-6, DOI: 10.1016/j.epsl.2014.09.001.

Large, W. G., and Pond, S., 1981. Open ocean momentum fluxes in moderate to strong winds. *Journal Physical Oceanography*, **11**: 324-336, DOI: 10.1175/1520-0485(1981)0112.0.CO;2.

Large, W. G., and Yeager, S. G., 2004. Diurnal to decadal global forcing for ocean and sea-ice models: The data sets and flux climatologies. *Technical Report TN–460+STR*. National Center for Atmospheric Research, Boulder, Colorado, 105pp.

Large, W. G., and Yeager, S. G., 2009. The global climatology of an interannually varying air-sea flux data set. *Climate Dynamics*, **33** (2-3): 341-364, DOI: 10.1007/s00382-008-0441-3.

Le, K., and Mao, H., 1990. Wintertime structures of temperature and salinity of the southern Huanghai (Yellow) Sea and its current systems. *Oceanologia et Limnologia Sinica*, **21**: 505-515 (in Chinese with English abstract).

Lin, C., Ning, X. R., Su, J. L., Lin, Y., and Xu, B., 2005. Environmental changes and the responses of the ecosystems of the Yellow Sea during 1976–2000. *Journal of Marine System*, **55**

(3-4): 223-234, DOI: 10.1016/j.jmarsys.2004.08.001.

Lin, X. P., Yang, J. Y., Guo, J. S., Zhang, Z. X., Yin, Y. Q., Song X. Z., and Zhang, X. H., 2011.An asymmetric upwind flow, Yellow Sea Warm Current: 1. New observations in the western Yellow Sea. *Journal of Geophysical Research*, **116** (C4): C04026, DOI: 10.1029/2010JC006513.

Lu, Y., and Stammer, D., 2004. Vorticity balance in coarse-resolution global ocean simulations. *Journal of Physical Oceanography*, **34**: 605-622, DOI: 10.1175/2504.1.

Mann, M. E., Steinman, B. A., and Miller, S. K., 2014. On forced temperature changes, internal variability, and the AMO. *Geophysical Research Letters*, **41** (9): 3211-3219, DOI: 10.1002/2014GL059233.

Park, K. A., Lee, E. Y., Chang, E. M., and Hong, S., 2015. Spatial and temporal variability of sea surface temperature and warming trends in the Yellow Sea. *Journal of Marine System*, **143**: 24-38, DOI: 10.1016/j.jmarsys.2014.10.013.

Park, S., Chu, R. C., and Lee, J. H., 2011. Interannual-to-interdecadal variability of the Yellow Sea Cold Water Mass in 1967–2008: Characteristics and seasonal forcings. *Journal of Marine System*, **87** (3-4): 177-193, DOI: 10.1016/j.jmarsys.2011.03.012.

Pörtner, H. O., Berdal, B., Blust, R., Brix, O., Colosimo, A., De Wachter, B., Giuliani, A., Johansen, T., Fischer, T., Knust, R., Lannig, G., Naevdal, G., Nedenes, A., Nyhammer, G., Sartoris, F. J., Serendero, I., Sirabella, P., Thorkildsen, S., and Zakhartsev, M., 2001. Climate induced temperature effects on growth performance, fecundity and recruitment in marine fish: Developing a hypothesis for cause and effect relationships in Atlantic cod (*Gadus morhua*) and common eelpout (*Zoares viviparus*). *Continental Shelf Research*, **21** (18-19): 1975-1997, DOI: 10.1016/S0278-4343(01)00038-3.

Qiao, L. L., Wang, X. H., Wang, Y. Z., Wu, D. X., Bao, X. W., and Lin, M., 2011. Winter heat budget in the Huanghai Sea and the effect from Huanghai Warm Current (Yellow Sea Warm Current). *Acta Oceanologica Sinica*, **30** (5): 56-63, DOI: 10.1007/s13131-011-0147-y.

Scaife, A. A., Arribas, A., Blockley, E., Brookshaw, A., Clark, R. T., Dunstone, N., Eade, R., Fereday, D., Folland, C. K., Gordon, M., Hermanson, L., Knight, J. R., Lea, D. J., MacLachlan, C., Maidens, A., Martin, M., Peterson, A. K., Smith, D., Vellinga, M., Wallace, E., Waters, J., and Williams, A., 2014. Skillful long-range prediction of European and North American winters. *Geophysical Research Letters*, **41** (7): 2514-2519, DOI: 10.1002/2014GL059637.

Song, D. H., Bao, X. W., Wang, X. H., Xu, L. L., Lin, X. P., and Wu, D. X., 2009. The inter-annual variability of the Yellow Sea Warm Current surface axis and its influencing factors. *Chinese Journal of Oceanology and Limnology*, **27** (3): 607-613, DOI: 10.1007/s00343-009-9159-2.

Stenevik, E. K., and Sundby, S., 2007. Impacts of climate change on commercial fish stocks in Norwegian waters. *Marine Policy*, **31** (1): 19-31, DOI: 10.1016/j.marpol.2006.05.001.

Stockdale, T. N., Molteni, F., and Ferranti, L., 2015. Atmospheric initial conditions and the predictability of the Arctic Oscillation. *Geophysical Research Letters*, **42** (4): 1173-1179, DOI: 10.1002/2014GL062681.

Sun, J., Gu, X. Y., Feng, Y. Y., Jin, S. F., Jiang, W. S., Jin, H. Y., and Chen, J. F., 2014. Summer and winter living coccolithophores in the Yellow Sea and the East China Sea. *Biogeosciences*, **11** (3): 779-806, DOI: 10.5194/bg-11-779-2014.

Tang, Y., Zou, E., and Lie, H. J., 2001. On the origin and path of the Huanghai Warm Current during winter and early spring. *Acta Oceanologica Sinica*, **23** (1): 1-12 (in Chinese with English abstract).

Taylor, K. E., 2001. Summarizing multiple aspects of model performance in a single diagram. *Journal of Geophysical Research*, **106** (D7): 7183-7192, DOI: 10.1029/2000JD900719.

Thompson, D. W. J., and Wallace, J. M., 1998. The Arctic Oscillation signature in the wintertime geopotential height and temperature fields. *Geophysical Research Letters*, **25** (9): 1297-1300, DOI: 10.1029/98GL00950.

Thompson, D. W. J., and Wallace, J. M., 2000. Annular modes in the extratropical circulation. Part I: Month-to-month variability. *Journal of Climate*, **13**: 1000-1016, DOI: 10.1175/1520-0442(2000)013<1000:AMITEC>2.0.CO;2.

Wagawa, T., Kuroda, T., Ito, S., Kakehi, S., and Yamanome, T., 2015. Variability in water properties and predictability of sea surface temperature along Sanriku coast, Japan. *Continental Shelf Research*, **103**: 12-22, DOI: 10.1016/j.csr.2015.04.016.

Wang, L., Chen, W., Zhou, W., and Huang, R. H., 2009a. Interannual variations of East Asian trough axis at 500 hPa and its association with the East Asian winter monsoon pathway. *Journal of Climate*, **22** (3): 600-614, DOI: 10.1175/2008JCLI2295.1.

Wang, L., Huang, R. H., Gu, L., Chen, W., and Kang, L. H., 2009b. Interdecadal variations of the East Asian winter monsoon and their association with quasi-stationary planetary wave activity. *Journal of Climate*, **22** (18): 4860-4872, DOI: 10.1175/2009JCLI2973.1.

Wang, L., Wei, H., and Batchelder, H. P., 2014. Individual-based modelling of Calanus sinicus population dynamics in the Yellow Sea. *Marine Ecology Progress Series*, **503**: 75-97, DOI: 10.3354/meps10725.

Wei, H., Shi, J., Lu, Y., and Peng, Y., 2010. Interannual and long-term hydrographic changes in the Yellow Sea during 1977–1998. *Deep Sea Research, Part II*, **57** (11-12): 1025-1034, DOI: 10.1016/j.dsr2.2010.02.004.

Wei, H., Yuan, C. Y., Lu, Y., Zhang, Z. H., and Luo, X., 2013. Forcing mechanisms of heat content variations in the Yellow Sea. *Journal of Geophysical Research*, **118** (9): 4504-4513, DOI: 10.1002/jgrc.20326.

Xu, Z. M., Song, X., Wang, M., Liu, Q., Jiang, Y., Shao, H. B., Liu, H. B., Shi, K. P., and Yu, Y., 2017. Community patterns and temporal variation of picoeukaryotes in response to changes in the Yellow Sea Warm Current. *Journal of Oceanography*, **73** (5): 687-699, DOI: 10.1007/s10872-017-0425-1.

Yu, F., Zhang, Z., Diao, X. Y., and Guo, J. S., 2010. The observation evidence of the Yellow Sea Warm Current. *Chinese Journal of Oceanography and Limnology*, **28** (2): 677-683, DOI: 10.1007/s00343-010-0006-2.

Yuan, C. Y., 2011. Forcing mechanisms of seasonal to decadal variations of oceanic temperature and circulation in the Yellow Sea. PhD thesis. Ocean University of China, Qingdao.

Zhang, S., Fei, Y., Diao, X. Y., and Guo, J. S., 2009. The characteristic analysis on sea surface temperature inter-annual variation in the Bohai Sea, Yellow Sea and East China Sea. *Marine Science*, **33**: 76-81 (in Chinese with English abstract).

Zhou, K. L., Sun, S., Wang, M. X., Wang, S. W., and Li, C. L., 2016. Differences in the physiological processes of *Calanus sinicus* inside and outside the Yellow Sea Cold Water Mass. *Journal of Plankton Research*, **38** (3): 551-563, DOI: 10.1093 plankt/fbw011.

(Edited by Xie Jun)